AGU PUBLICATIONS

JGR

Journal of Geophysical Research: Solid Earth

RESEARCH ARTICLE
10.1002/2015JB012135

Key Points:
- Stratigraphic and subsurface data indicate existence of growth strata
- New magnetostratigraphy constrains the inception of growth strata at ~6.4 Ma
- Quaternary deformation is revealed by geomorphologic data

Correspondence to:
H. Lu,
hhlv@geo.ecnu.edu.cn

Citation:
Lu, H., Z. Wang, T. Zhang, J. Zhao, X. Zheng, and Y. Li (2015), Latest Miocene to Quaternary deformation in the southern Chaiwopu Basin, northern Chinese Tian Shan foreland, *J. Geophys. Res. Solid Earth*, *120*, 8656–8671, doi:10.1002/2015JB012135.

Received 20 APR 2015
Accepted 13 NOV 2015
Accepted article online 17 NOV 2015
Published online 12 DEC 2015

Latest Miocene to Quaternary deformation in the southern Chaiwopu Basin, northern Chinese Tian Shan foreland

Honghua Lu[1], Zhen Wang[1], Tianqi Zhang[1,2], Junxiang Zhao[3], Xiangmin Zheng[1], and Youli Li[4]

[1]School of Geographic Sciences, East China Normal University, Shanghai, China, [2]Now at Institute of Earth and Environmental Science, University of Potsdam, Potsdam, Germany, [3]Institute of Crustal Dynamics, China Earthquake Administration, Beijing, China, [4]Key Laboratory of Earth Surface Processes of Ministry of Education, Peking University, Beijing, China

Abstract Basinward propagation of fold and thrust belts is a crucial geological process accommodating Cenozoic crustal shortening within the India-Eurasia collision zone. Anticlinal growth strata in the southern Chaiwopu Basin (a piggyback basin) of the northern Chinese Tian Shan foreland record basinward encroachment of the Tian Shan along the Junggar Frontal Thrust Fault. A new magnetostratigraphic section constrains the onset of syntectonic growth strata at circa 6.4 Ma and suggests synchronous basinward thrusting and propagation of the Tian Shan. The intense alluviation in the southern Chaiwopu Basin ceased at circa 0.55 Ma due to significant anticlinal growth and its resultant river incision. More recent anticlinal growth and deformation during the late Quaternary are revealed by folded river terraces developing across the anticline. The terrace height profile indicates that terrace T_1^H has been vertically offset about 0.6 m by thrust faulting since its formation at about 7 Ka. The stratigraphic and geomorphic data presented in this work are helpful to understand the initiation of thrust-related folding, as well as aggradation and subsequent incision, in foreland basins of the Tian Shan in relation to the India-Asia collision.

1. Introduction

Since the early Cenozoic, the India-Asia collision has driven deformation exerting a dominant control on the tectonic and topographic patterns of central Asia, including western China [*Najman et al*., 2001; *Zhang*, 2004] (Figure 1a). As a result of the collision, the Tian Shan (Shan means "mountains" in Chinese) has been tectonically reactivated and intensely uplifted as crustal shortening propagated into its foreland basins [*Windley et al*., 1990; *Avouac et al*., 1993; *Yin et al*., 1998; *Deng et al*., 2000]. The well-exposed rocks in and adjacent to the arid to semiarid Tian Shan provide an ideal natural laboratory where the temporal and spatial history of tectonic deformation caused by the India-Asia convergence can be unraveled with exceptional clarity. Previous studies of the timing and magnitude of the Cenozoic tectonic deformation of the Tian Shan have utilized low-temperature thermochronology [e.g., *Hendrix et al*., 1994; *Bullen et al*., 2003; *Sobel et al*., 2006a, 2006b; *Lu et al*., 2013a; *Yu et al*., 2014], magnetostratigraphy [e.g., *Chen et al*., 2002, 2007; *Charreau et al*., 2005, 2006; *Heermance et al*., 2007, 2008; *Sun et al*., 2009; *Lu et al*., 2010a; *Thompson et al*., 2015], geological and geodetic investigations [e.g., *Reigber et al*., 2001; *Zubovich et al*., 2010], or geomorphologic data [e.g., *Avouac et al*., 1993; *Burchfiel et al*., 1999; *Fu et al*., 2003; *Scharer et al*., 2006; *Lu et al*., 2010b; *Yang et al*., 2012; *Li et al*., 2013]. Nonetheless, the detailed character, sequence, and magnitude of the structural, depositional, and geomorphic responses to the ongoing collision contain many gaps. Here we provide new stratigraphic and geomorphic data on the initiation of thrust-related folding, as well as aggradation and subsequent incision within a piggyback basin (i.e., the Chaiwopu Basin) of the northern Chinese Tian Shan foreland.

The Chaiwopu Basin is situated in the easternmost part of the northern Chinese Tian Shan foreland (Figures 1a and 1b). Geomorphologically and tectonically, the basin lies in the transitional zone of the eastern Tian Shan (Bogda Shan and Balikun Shan) and the western Tian Shan: a diffuse N-S boundary which generally lies near the city of Urumqi (Figures 1a and 1b). Given its position at this transition, the Chaiwopu Basin is thus a key area to understanding the late Cenozoic deformation of the Tian Shan. At the southern margin of the basin, the small-scale Saerqiaoke anticline dominates the local topography [*Lu et al*., 2014] (Figures 1b and 1c). This anticline is causally linked with basinward thrusting along the north branch of southern Chaiwopu Fault (NSCF), which branches from the Junggar Frontal Thrust Fault (JFTF) bounding the northern Tian Shan and its foreland basin [*Liu et al*., 2007]. However, the history of anticlinal growth and deformation

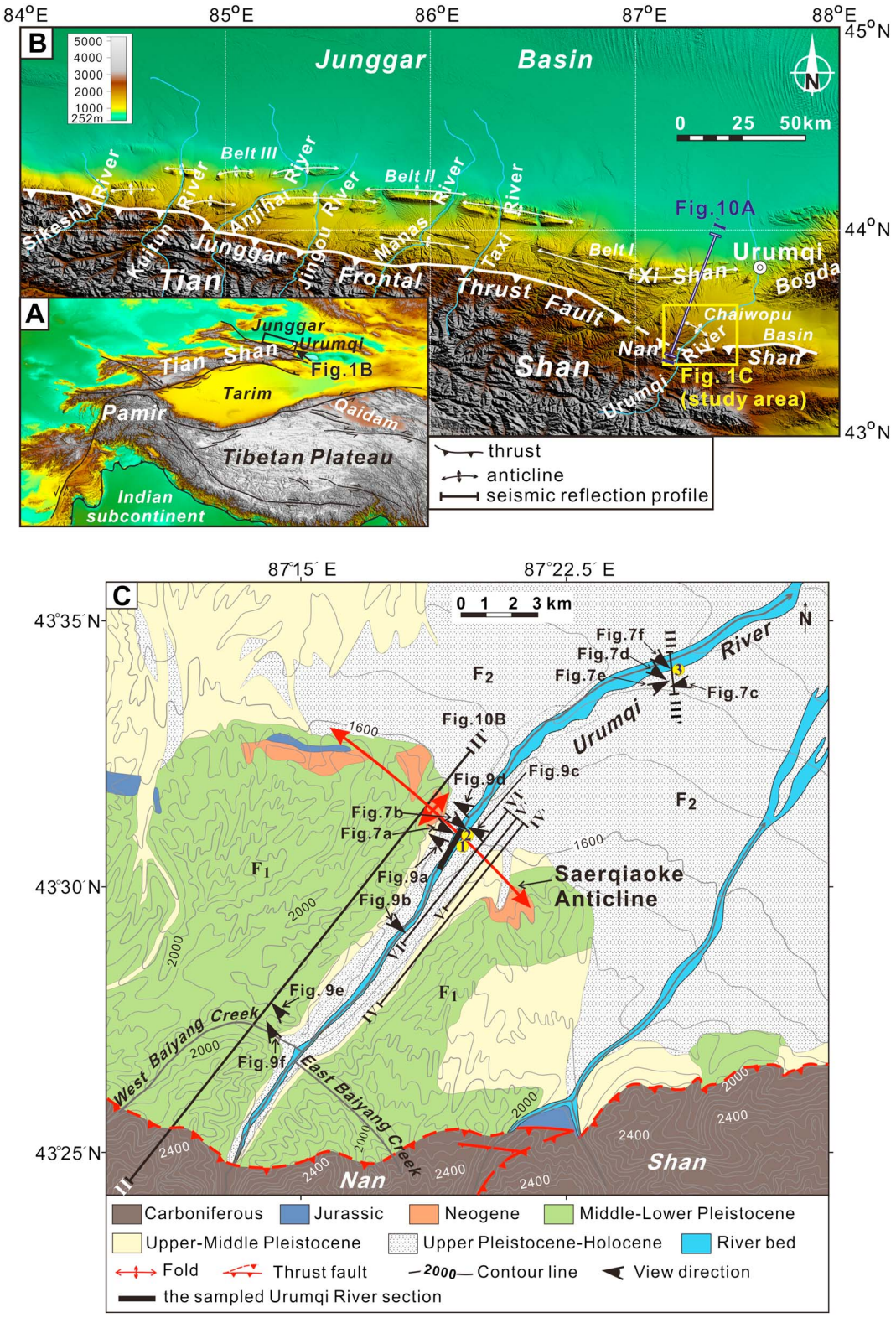

Figure 1. (a) Map shows tectonic setting and topographical pattern of the Indian-Eurasian convergence zone. (b) Digital elevation model of the northern Chinese Tian Shan foreland where fold and thrust belts I to III characterize the regional topography. (c) Geological map in the southern Chaiwopu Basin where thick Quaternary alluviums deposited as alluvial fans F_1 and F_2 of the Urumqi River. Circles with numbers show the sampling sites for optically stimulated luminescence (OSL) dating, as reported in Table 1.

remains unclear, with little stratigraphic and geomorphic evidences to precisely date the late Cenozoic tectonic activity in the southern Chaiwopu Basin.

In foreland basins, detailed sedimentological and geomorphological investigations are helpful to understand the tectonic evolution of the basin [e.g., *Molnar et al*., 1994; *Burbank et al*., 1996; *Burchfiel et al*., 1999; *Burbank and Anderson*, 2011; *Yang and Li*, 2011; *Yang et al*., 2014; *Thompson et al*., 2015]. The main aim of this work is to develop a chronology of the late Cenozoic deformation in the southern Chaiwopu Basin of the northern Chinese Tian Shan foreland by integrating stratigraphic and geomorphic data. Our results help to reveal the activity of major faults in the basin and further to understand their seismic behavior: a focus that is significant given the active deformation and high seismicity in the modern Tian Shan and its foreland basins [*Deng et al*., 2000; *Reigber et al*., 2001].

2. Geological Background

As one of the largest and most active orogenic belts in the Asia inland, the EW-trending Tian Shan has experienced a complex geological history. Previous studies [e.g., *Windley et al*., 1990; *Yin et al*., 1998; *Deng et al*., 2000] have revealed that the ancestral Tian Shan arose from several block collisions during the Late Devonian-Early Carboniferous and Late Carboniferous-Early Permian, along with the formation of a suite of EW-trending strike-slip and thrust faults (Figure 1a). The Mesozoic deformation of the range was dominated by relative tectonic stability during the Triassic-Late Jurassic, followed by active deformation during the Late Jurassic-Early Cretaceous [*Lu et al*., 2010a]. The subsequent relative stability during the latest Mesozoic-Paleogene caused the beveling of topography within the Tian Shan [*Allen et al*., 1991; *Bullen et al*., 2003]. As a result of the Cenozoic India-Asia collision, the Tian Shan range has been tectonically reactivated and gradually encroached into its foreland basins [*Deng et al*., 2000; *Lu et al*., 2010a, 2013a]. In the northern Chinese Tian Shan foreland, such a geological process has formed three fold and thrust belts known as belts I to III that characterize the regional topography (Figure 1b).

Situated in the easternmost part of the northern Chinese Tian Shan foreland, the Chaiwopu Basin is separated from the Junggar Basin to the northwest by the Xi Shan (i.e., the easternmost part of fold and thrust belt I) (Figure 1b), a low mountain range with elevations of 1–2 km. The basement rocks of the Chaiwopu Basin comprise Permian to Triassic strata [*Gao*, 2004]. The basin fill consists of Tertiary and Quaternary strata. The Tertiary comprises the Donggou Group (Cretaceous-Eocene) and the Manas (Oligocene), Qianshan (Miocene), and Changjihe (Pliocene) Formations, and the lithology is dominated by lacustrine mudstone, sandstone, and conglomerate. In general, the basement rocks and Tertiary strata are exposed on both the southern and northern margins of the Chaiwopu Basin due to tilting, thrusting, and folding. The overlying Quaternary strata are massive alluvial conglomerates. Where the Urumqi River flows into the lowland southern Chaiwopu Basin, two episodes of Quaternary alluvial fan deposition (the fans F_1 and F_2) are apparent [*Lu et al*., 2014] (Figure 1c). Stratigraphically, the fan F_1 conglomerates (designated as Saerqiaoke Gravel by *Zhou et al*. [2002]) is equivalent to Urumqi Gravel, an early-middle Pleistocene succession of thick fluviatile conglomerates deposited as a part of the basin fill in the northern Chaiwopu Basin [*Gao*, 2004]. Progressive incision into the fans F_1 and F_2 by the Urumqi River has created a well developed flight of terraces [*Lu et al*., 2014].

3. Methodology

In a fault-bounded foreland basin like the Chaiwopu Basin, the investigations of both tectono-sedimentary evolution and geomorphic expression of tectonic deformation are crucial to reveal the history of tectonic deformation of the basin [e.g., *Burbank*, 1992; *Burbank et al*., 1996; *Bullen et al*., 2003; *Chen et al*., 2007; *Heermance et al*., 2007; *Lu et al*., 2010a; *Burbank and Anderson*, 2011; *Vandenberghe et al*., 2011; *Yang et al*., 2012, 2014]. Certainly, such analysis should be placed in a robust temporal framework. We thus conducted a magnetostratigraphic investigation in order to date the basin fill. Correspondingly, our work comprises two principal facets: (i) stratigraphic and magnetostratigraphic analysis and (ii) geomorphologic investigation.

3.1. Stratigraphic and Magnetostratigraphic Analysis

The continuous growth and uplift of a structure (such as a fault-related fold) are capable of causing a distinct geometry of sediments progressively depositing above this structure, and correspondingly, the stratigraphy is described as growth strata (i.e., syntectonic sedimentation) [e.g., *Suppe et al*., 1992; *Burbank et al*., 1996;

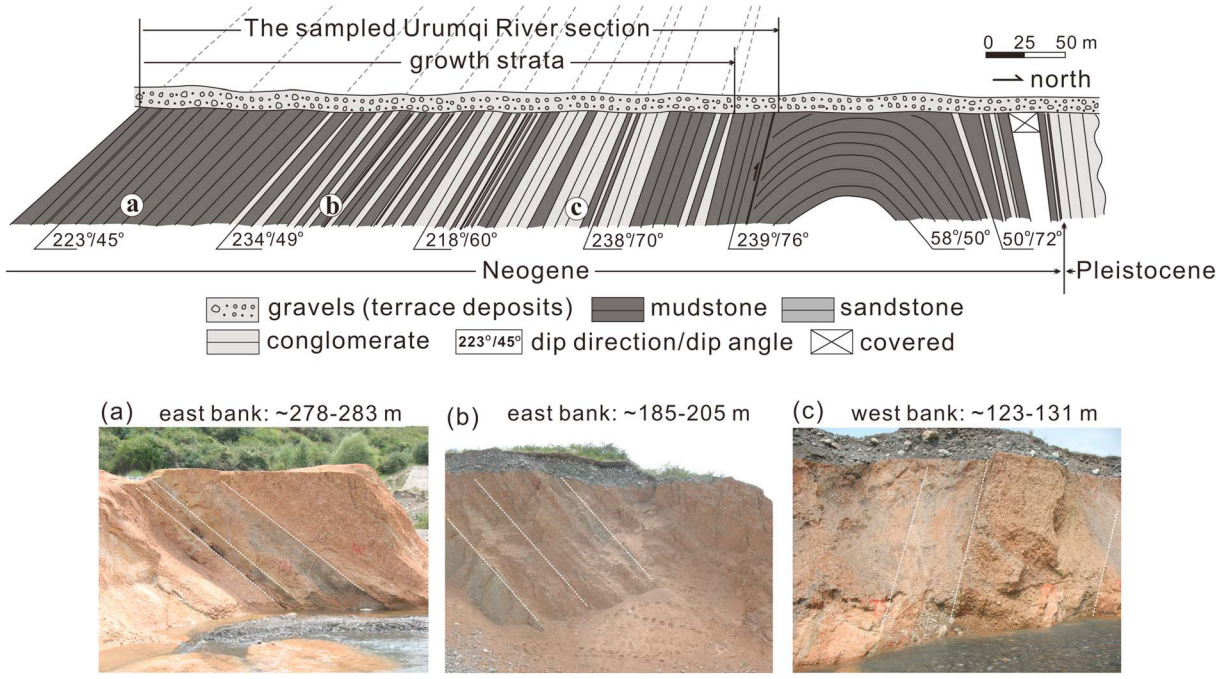

Figure 2. Measured geological section across the Saerqiaoke anticline exposed by the Urumqi River. (a–c) The representative lithofacies. "~278–283 m" shows the stratigraphic level in the measured Urumqi River section (URS). The first significant change in dip angle in the URS is interpreted to represent inception of syntectonic growth strata. The labeled fault in the URS is a branch of the north branch of southern Chaiwopu Fault (NSCF).

Heermance et al., 2007]. Thus, we reconstructed the local tectonic evolution by studying the geometry of the sedimentary strata in the southern Chaiwopu Basin, and this reconstruction is based mainly on the following two lines of investigations. In the field, we extensively investigated the stratigraphic contacts, took detailed measurements of bedding attitudes, and described the lithofacies. We also analyzed a seismic reflection profile through the Saerqiaoke anticline which was reported by *Liu et al*. [2007].

In order to date the basin fill, we sampled a magnetostratigraphic section in the upper Cenozoic terrigeneous sequence, exposed across the southern limb of the Saerqiaoke anticline by the Urumqi River (Figure 1c) and hereafter referred to as the "Urumqi River section (URS)". The sampled URS is about 310 m thick (Figure 2). Lithologically, the section comprises mainly brownish yellow/red mudstone, but the middle part of the section is dominated by interbedded brown/gray conglomerates and mudstone (Figure 2). This lithofacies association is interpreted to define an alluvial-lacustrine depositional system, a sedimentary environment developing in the northern Chinese Tian Shan foreland during the periods of Neogene-Quaternary [e.g., *Charreau et al*., 2005; *Lu et al*., 2010a]. The absence of significant observable faulting or major erosional discordance suggests no significant depositional breaks in the URS, i.e., a relatively continuous sedimentary process.

3.2. Geomorphologic Investigation

Deformed river terraces and alluvial fan surfaces can be used to reconstruct the recent tectonic evolution in the basin margin [e.g., *Molnar et al*., 1994; *Burchfiel et al*., 1999; *Burbank and Anderson*, 2011; *Yang and Li*, 2011]. The fluvial geomorphologic classification in the southern Chaiwopu Basin has been reported in our recent work [*Lu et al*., 2014]. In this paper, we determine the timing and magnitude of the anticlinal deformation by characterizing the deformed terraces across the Saerqiaoke anticline. The longitudinal profiles of terraces are used to reveal the Quaternary deformation in relation to the fold growth. Such profiles were extracted from Google Earth images except the terrace height profile of T_1^H that was measured with TruPulse 200. The ages of the high terraces are from our previous study [*Lu et al*., 2014], and the formation ages of the low terraces reported in this paper were dated by optically stimulated luminescence (OSL) dating method. Samples for OSL dating were taken by inserting a 20 cm long, 5 cm diameter steel pipe with one end covered with opaque materials into the sampled layer. In order to ensure maximal shielding, only the middle part of each sample was analyzed. The OSL dates were determined in the Institute of Crustal Dynamics of

China Earthquake Administration following the procedures of *Rees-Jones* [1995] and *Wang* [2006]. We have also investigated the geomorphology of the area beyond the Saerqiaoke anticline to identify the transition of downcutting and deposition of the Urumqi River.

4. Magnetostratigraphy of the Urumqi River Section

4.1. Paleomagnetic Sampling and Lad Measurements

In the Urumqi River section, paleomagnetic sampling yielded 82 sampling horizons from which a total of 184 specimens were collected. We drilled specimens with an average interval of about 3.7 m varying between 0.2 and 6.5 m. The specimens were collected from mudstone, siltstone, or fine-grained sandstone. The orientations of all the specimens were measured with a magnetic compass corrected by the local magnetic declination (4.8°E at the URS sampling site).

One specimen per sampling horizon was subjected to stepwise (13–17 steps) thermal demagnetization. For the stratigraphic horizons where measured specimens showed unstable high-temperature demagnetization trajectories, a second specimen was selected for another round of thermal demagnetization. Generally, thermal demagnetization intervals are 50–80°C below 500°C, 25°C or 35°C between 500 and 610°C, and 10–20°C above 610°C. Magnetic remanence was measured with a 2G-755 cryogenic magnetometer installed in magnetic-free space (<300 nT) at the Institute of Geology and Geophysics, Chinese Academy of Sciences, Beijing. The characteristic remanent magnetization (ChRM) directions of the measured specimens were determined by principal component analysis [*Kirschvink*, 1980], and the identified directions were further analyzed with Fisher statistics [*Fisher*, 1953]. The directions (magnetic declination and inclination) of the selected specimens were used to calculate virtual geomagnetic pole (VGP) latitudes. The magnetic polarity stratigraphy (MPS) was finally constructed using the VGP data for the sampled URS and then correlated to the geomagnetic polarity time scale (GPTS) of *Lourens et al*. [2004] to constrain the age of the URS.

4.2. Demagnetization

The natural remanent magnetization is between 0.381×10^{-5} A/m and 12.0×10^{-5} A/m with an average of $3.26 \pm 2 \times 10^{-5}$ A/m. Stepwise thermal demagnetization successfully isolated dominant magnetic components for most of the analyzed specimens after eliminating the viscous remanent magnetization, whereas a few specimens exhibited scattered demagnetization directions which we did not use for the subsequent analysis. For the specimens exhibiting relatively stable high-temperature demagnetization trajectories, the maximum angular deviation was between 4.5° and 14.9° with an average of 12.4 ± 4.4°. The decay curves during demagnetization and Zijderveld plots indicate that their demagnetization behaviors contain three main magnetic components (Figure 3): the low-temperature component (LTC) between 0°C and 250–300°C representing ~30–40% of the total remanence, the intermediate temperature component (ITC) between 250–300°C and 500–525°C representing ~25–40% of the total remanence, and the high-temperature component (HTC) in a temperature range extending from ~500 to 525°C to commonly 610 or rarely 680°C representing ~20–45% of the total remanence. For the HTC of the most specimens, the magnetic carrier is most likely magnetite or titanomagnetite, as indicated by the sharp decrease in remanence occurring between 525 and 580°C (Figures 3a, 3b, and 3c). The HTC of a few specimens is likely carried by hematite or maghemite that revealed by the significant drop in remanence between 610 and 680 C (Figure 3d) [*Butler*, 1992].

4.3. Reversal and Fold Tests

Reversal and fold tests are commonly used to determine whether acquisition of the ChRM directions is predeformation, syndeformation, or postdeformation. Figure 4 shows that tilt correction improves the grouping of ChRM poles of the URS. The Fisherian site-averaged normal and reversed polarity poles have an observed angular difference of 5.98°. This angular difference is smaller than the critical angle of 12.11° at the 95% confidence level and on the basis of the assumed identical dispersion K, implying that the URS passes the C-class reversal test [*McFadden and McElhinny*, 1990]. Due to poor outcrop preservation, only a few oriented specimens were collected from the northern limb of the Saerqiaoke anticline to perform the standard fold test. Instead, the simple fold test of *McElhinny* [1964] was employed with the specimens from the URS in the fold's southern limb (Figure 4). The results show that the K_{crit} values of 1.60 (normal polarity) and 1.47 (reversed polarity) are respectively smaller than the K_s/K_g ratios of 1.64 (normal) and 1.53 (reversed)

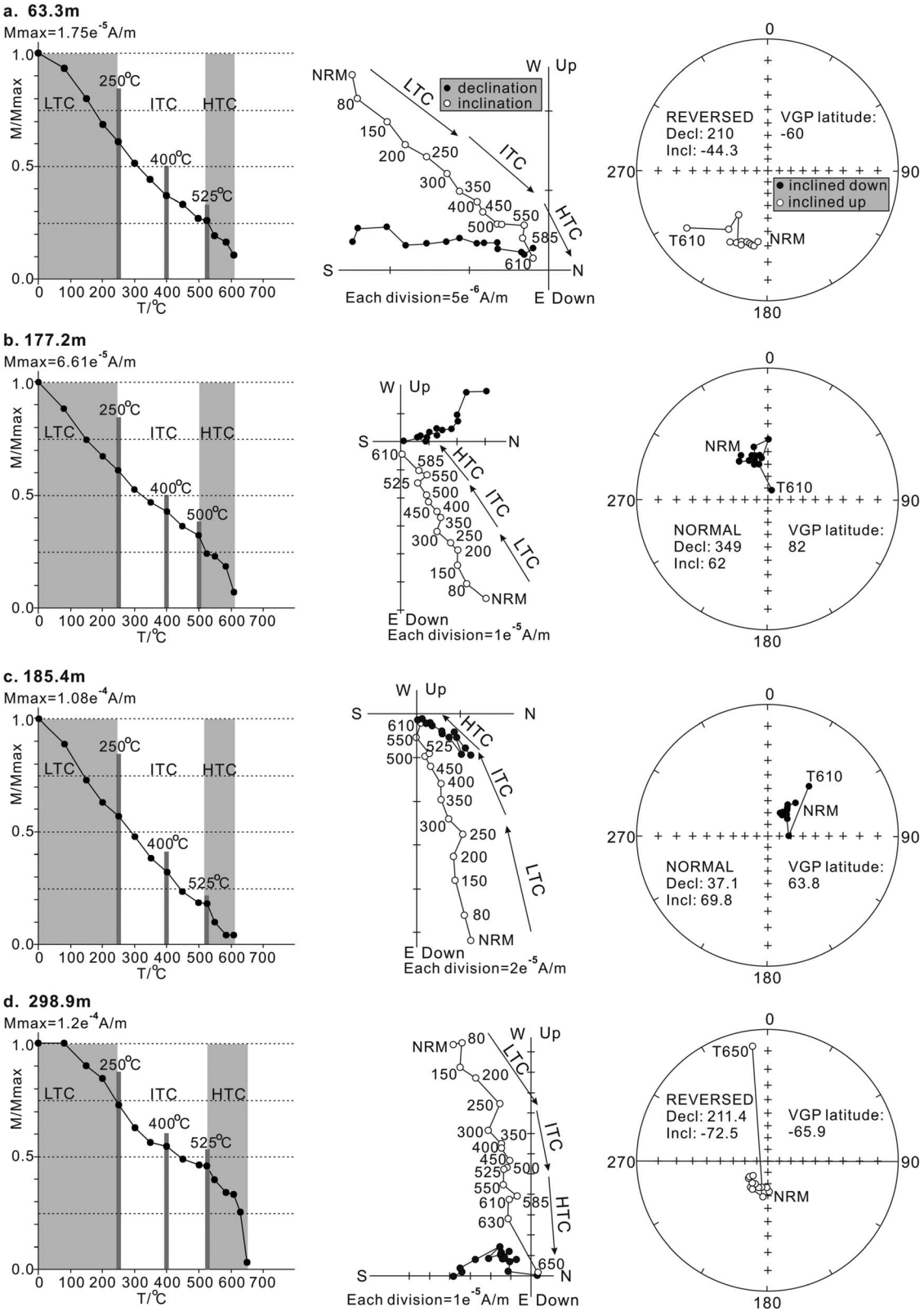

Figure 3. Representative thermal demagnetization plots typically showing two or three magnetic components. The low-temperature component (LTC), the intermediate temperature components (ITC), and the high-temperature component (HTC) of the characteristic remanence magnetization (ChRM) are depicted for each selected sample. (left column) Remanent magnetic intensity graphs; (center column) Zijderveld diagrams; and (right column) Equal-area projections. 300 = 300°C. "63.3 m" indicates the sampling stratigraphic level of the measured specimen in the Urumqi River section.

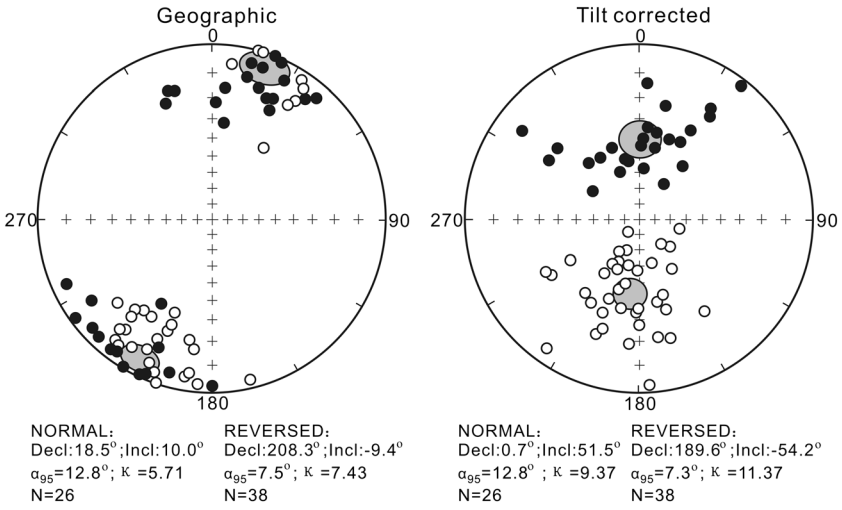

Figure 4. Stereonet plots of palaeomagnetic data from the URS. Small solid (inclined down) and white (inclined up) circles indicate individual measurements with the larger circles showing the α_{95} error around the Fisher mean. The Fisher mean data are listed adjacent to each plot.

at the 95% confidence level. Here K_s and K_g are the dispersions in the stratigraphic and geographic coordinates, and K_{crit} is defined as the *f* distribution with $2(N-1)$ degrees of freedom, where *N* is the amount of specimens with a specified magnetic polarity. The above results suggest a positive fold test [*McElhinny*, 1964]. Thus, the positive reversal and fold tests (Figure 4) imply that the ChRM directions of the URS sediments were acquired before deformation.

4.4. Magnetic Polarity Stratigraphy

The ChRM directions of all the accepted specimens were determined by least squares fitting through the temperature points commonly above 450°C (minimum of three but more typically four to six). The determined ChRM directions were then used to calculate the VGP latitudes. When constructing the MPS for the URS, specimens with VGPs $<30°$ were not used except when they displayed the same polarity with the adjacent specimens showing VGPs $\geq 30°$. However, a single specimen with VGP $\geq 30°$ was not considered if its adjacent specimens display the opposite polarity. The ChRM vector directions of a total of 64 specimens were used to define the MPS of the URS, which contains 13 magnetozones (Figure 5). Each magnetozone is defined by at least two specimens with VGPs $\geq 30°$. Two zones (n1 and n2) are less certain because they include only one specimen with VGP $\geq 30°$. Overall, five normal (N1-N5) and four reversed (R2-R5) magnetozones are clearly identified in the URS column.

Our magnetostratigraphy was then correlated to the GPTS of *Lourens et al*. [2004] (Figure 5) based on the following observations: (1) one interval with a distinctive pattern of local magnetic polarity (N1-N4), which is interpreted as the Gilbert polarity chron; (2) one relatively long reversed magnetozone (R5); (3) the relatively continuous depositional process throughout the section without significant depositional breaks; and (4) the possible age of Mio-Pliocene of the sampled URS sediments. On the basis of the vertebrate fauna containing *Equus sanmeniensis* (horse) as well as the preliminary magnetostratigraphic result, the upper boundary of Urumqi Gravel in the northern Chaiwopu Basin is inferred to lie slightly above the Brunhes-Matuyama paleomagnetic boundary (i.e., <0.78 Ma) [*Gao*, 2004]. Its lower boundary is inferred to be not older than about 1.87 Ma [*Li et al*., 1990; *Gao*, 2004]. Stratigraphically, Urumqi Gravel corresponds to Saerqiaoke Gravel (i.e., the fan F_1 conglomerates) in the southern Chaiwopu Basin, implying that these two stratigraphic units have a similar age. Detailed field observations show that the relatively gently inclined layers of Saerqiaoke Gravel overlie the sampled URS sediments (see Figure 10b). This observed superposition suggests the URS is likely upper Neogene.

Overall, our preferred correlation matches the main patterns of magnetic polarity reversal in the Latest Miocene to Pliocene GPTS [*Lourens et al*., 2004] (Figure 5). Of course, some ambiguities remain with this correlation, e.g., normal magnetozones n1 and n2. We matched n1 and n2 with the subchrons C2An.3n

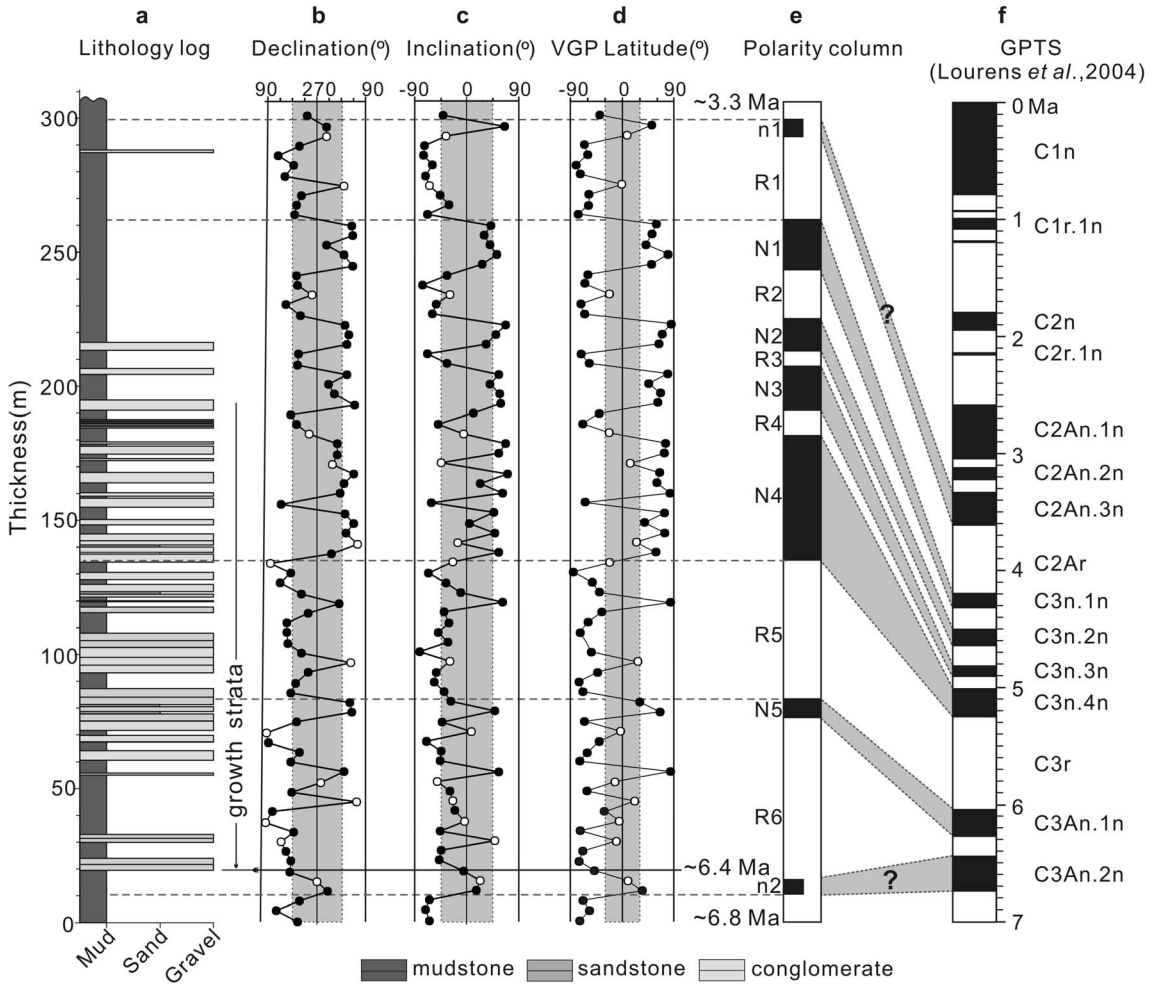

Figure 5. Magnetic polarity stratigraphy (MPS) of the Urumqi River section. (a) Lithology log with the base of growth strata dated at about 6.4 Ma. (b) Magnetic declination in tilt-corrected coordinates (shaded zone equals 180°–360°). (c) Magnetic inclination in tilt-corrected coordinates (shaded zone equals ±45°). (d) Virtual geomagnetic pole (VGP) latitude (shaded zone equals ±30°). Open circles represent specimens with absolute values of VGPs <30°, which were not used to define the MPS of the URS, except for the local magnetozones n1 and n2. (e) Magnetic polarity stratigraphy defined commonly by specimens with absolute values of VGPs ≥30°. Black and white zones indicate normal and reversed polarity, respectively. Boundaries between magnetozones are defined by the midpoint between two specimens with opposite polarity. Magnetozones (n1 and n2) defined only by two specimens with one showing VGP <30° are displayed by short-half bars. (f) Reference geomagnetic polarity time scale (GPTS) of *Lourens et al.* [2004].

and C3An.2n, respectively, based mainly on the correlation of the magnetozones N1-N5 with the subchrons C3n.1n-C3An.1n (Figure 5). Despite inevitable uncertainties, the correlation, especially between the magnetozones N1-N5 and the subchrons C3n.1n-C3An.1n of the GPTS [*Lourens et al.*, 2004], appears acceptable. Our above correlation thus constrains the basal age of the sampled URS to about 6.8 Ma, spanning from ~6.8 to ~3.3 Ma (Figure 5). Based on this correlation, the relationship between the thickness and magnetostratigraphic ages of the URS sediments shows two decreases in the sediment-accumulation rate at about 6.1 and 4.1 Ma (Figure 6), with an average rate of ~95 m/Myr over the 3.5 Myr interval of the URS.

5. Geomorphologic Observations

In our recent work, nine terraces (T_1 to T_9, increasing systematically in elevation) have been identified in the southern Chaiwopu Basin (Figure 7a) [*Lu et al.*, 2014]. Field investigations suggest that terraces T_9, T_7, T_5, and T_4 are the best expressed fluvial features in this area, and terraces T_9 and T_4 correspond to alluvial fans F_1 and F_2, respectively. Above the core of the Saerqiaoke anticline, terrace T_1 can be divided to the high terrace T_1^H and the low terrace T_1^L based on the terrace height above the riverbed (Figures 1c and 7a). Our new OSL

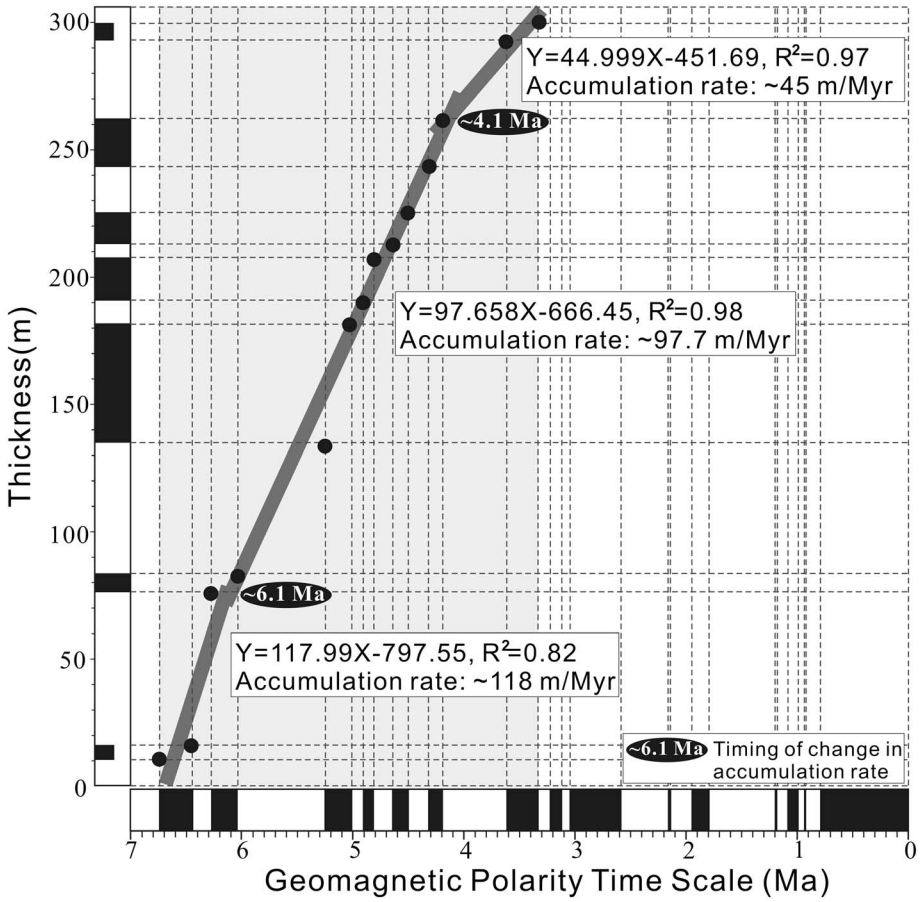

Figure 6. Age versus thickness plot of the Urumqi River section showing changes in sediment-accumulation rate at about 6.1 and 4.1 Ma, respectively.

dating data (Table 1) constrain the formation age of terraces T_1^H and T_1^L to ~7 Ka and ~2 Ka, respectively. The formation age or depositional age of the older terraces have been determined by electron spin resonance dating method [*Lu et al.*, 2014]: the abandonment of terrace T_9 (i.e., fan F_1) was dated at about 0.55 Ma; the depositional age of terrace T_7 was constrained to about 0.26 Ma; and terrace T_5 is estimated to have formed at about 0.14 Ma.

About 10 km northeast of the distal end of F_1 (Figure 1c), the downcutting into the alluviums of fan F_2 has yielded four terraces well developed along the course of the Urumqi River (Figures 7c to 7f). Based mainly on surface characteristics, elevations above the modern riverbed, terrace deposits and the depositional age of the lowest terrace (about 6 Ka, Table 1), these four terraces were classified as T_1 to T_4 (Figure 8a). It is clear that the terrace deposits of the three younger terraces (T_1 to T_3) overlie the fan F_2 conglomerates (Figures 7c to 7f and 8a).

Here we focus on the deformation of terraces T_7, T_5, T_4, and T_1^H (Figures 7b and 8b). In response to significant rock uplift of the fold, terraces T_7, T_5, and T_4 have been created as strath terraces [see *Lu et al.*, 2014, Figure 5]. The longitudinal profiles indicate that these three terraces have been significantly warped up over the Saerqiaoke anticline (Figure 8b). In more extensive areas beyond this anticline, old terraces (here they are terraces T_7 and T_5) have been buried due to accumulation of younger alluvial sediments caused by relative subsidence (Figure 8b). Subsequent river incision has formed young fill terraces (like T_4 to T_1) in these areas. Here it is unlikely to quantitatively estimate the magnitude of deformation of terraces T_7 and T_5 due to the burial (Figure 8b). It is clear that, however, the older terraces record more deformation (Figure 8b). The more recent deformation of the Saerqiaoke anticline is recorded by the young terrace T_1^H (Figures 1c and 7b). In the anticlinal core, a branch of NSCF controlling the fold growth, which has the dip direction of ~215°

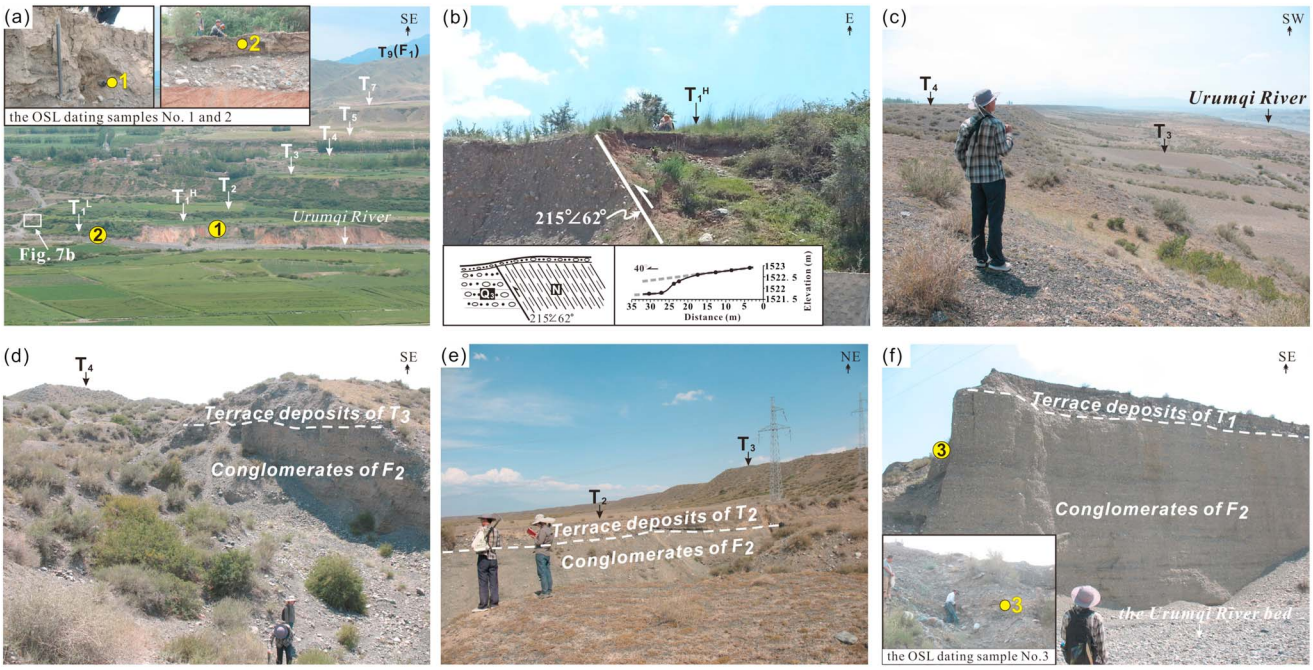

Figure 7. (a) Alluvial sequence developed by the Urumqi River in the southern margin of the Chaiwopu Basin. (b) The deformed terrace T_1^H, with the insert showing the magnitude of thrust faulting of about 60 cm determined by the measured terrace height profile. (c–f) Photos showing the geomorphic structure of four terraces that developed owing to the downcutting into the alluviums of fan F_2 about 10 km northeast of the distal end of F_1. In Figures 7a and 7f, the inserts show the sections from which the OSL dating samples were taken. See Figure 1c for the locations and view directions of these photos.

and the dip angle of ~62°, reaches the surface between the terrace deposits of T_1^H and the underlying strata of Neogene and upper Pleistocene on the east bank of the Urumqi River (Figure 7b). It has thrust the Neogene mudstone northward onto the upper Pleistocene conglomerates and has offset the terrace surface of T_1^H. The measured terrace height profile transverse to the thrust scarp indicates that terrace T_1^H has been vertically offset about 0.6 m by the thrust (Figure 7b).

6. Discussion

6.1. Northward Propagation of the Tian Shan at ~6.4 Ma

In foreland basins, variations in lithofacies and rates of sediment accumulation could reveal local tectonic activity [e.g., *Meigs et al*., 1995; *Lu et al*., 2010a]. However, these changes could also be forced by nontectonic factors, including source lithology, transport distance [*DeCelles and Giles*, 1996], and paleoclimate [*Molnar*, 2001, 2004; *Zhang et al*., 2001; *Dupont-Nivet et al*., 2007]. Thus, the sediments, such as conglomeratic facies, cannot serve as definitive records of tectonic deformation within a foreland basin. In contrast, growth strata, i.e., syntectonic sedimentation, can indicate a direct link to growth and uplift of a structure, such as a fault-related fold [*Riba*, 1976; *Suppe et al*., 1992; *Burbank et al*., 1996]: its continuous growth can cause a characteristic wedge-shaped, syntectonic geometry of the sediments depositing over the structure [*Burbank et al*., 1996].

Field observations on stratigraphic geometry of Neogene-Pleistocene (Figures 2, 9, and 10b) reveal the existence of growth strata that reflect the syndepositional growth of the Saerqiaoke anticline in relation to the NSCF. Systematic changes in bedding dips were observed on both limbs of the Saerqiaoke anticline. In the fold's southern limb, the Neogene strata close to the anticlinal core dip to the southwest at an angle $>30°$ (Figures 9a and 10b). The attitude of the overlying F_1 conglomerates (i.e., Saerqiaoke Gravel) is concordant with the Neogene strata (Figure 10b). About 4 km to the south, the dips of Saerqiaoke Gravel exposed in the Urumqi River valley decrease to $<10°$ (Figures 9b and 10b). Wherever these two stratal units are juxtaposed close to the anticlinal core in Saerqiaoke's northern limb, the dip angle of Saerqiaoke Gravel gradually decreases upward from near vertical in the Urumqi River valley (Figures 9c and 10b) to ~45° near the top of

Table 1. Calculated Values of Equivalent Doses, Annual Doses, and OSL Ages [a]

Sample No.	Sampled Layer (m)	U (μg/g)	Th (μg/g)	K (%)	Water Content (%)	Equivalent Doses (Gy)	Annual Doses (Gy/kyr)	OSL Age (ka) [b]
1[c]	At the base of ~90 cm thick silt above the ~1.9 m thick terrace gravels of T_1^H. The terrace height above the current riverbed is about 19.6 m.	2.52	10.6	2.33	3.36	4.64	35.76 ± 1.66	7.70 ± 0.85
2	At the depth of 40 cm in the 80 cm thick silt very fine sand of T_1^L. The terrace gravels is about 2.2 m thick and the terrace height above the riverbed is about 8.4 m.	2.43	12	2.20	2.57	4.65	10.57 ± 0.50	2.28 ± 0.25
3	At the depth of 4.3 m in the ~4.6 m thick terrace gravels of T_1. The sampled layer is ~20 cm thick very fine sand and the terrace height above the riverbed is about 12 m.	1.36	6.71	2.35	0.34	3.77	21.98 ± 1.46	5.83 ± 0.70

[a]The dating technique is Sensitivity-corrected Multiple Aliquot Regenerative-dose, and the dating material is quartz (4–11 μm).
[b]The age uncertainty is 1 σ.
[c]Locations of dating samples and sampled sections are shown in Figures 1, 7a, and 7f, respectively.

the alluvial fan F_1 (Figures 9d and 10). Steeper strata were observed on the forelimb of this fold (Figures 2 and 10b), indicating its asymmetric structure. The measured URS in Saerqiaoke's southern limb further reveals the geometry of sedimentary strata composing the Saerqiaoke anticline. In general, the stratal dips in the URS gradually decrease upward from about 80° at the base of the section (close to the anticlinal core) to about 45° at its top (away from the anticlinal core) (Figures 2 and 10b).

The above observations on stratal attitudes indicate a characteristic wedge-shaped stratigraphic geometry of the strata composing Saerqiaoke's limbs (Figure 2 and 10b), consistent with syntectonic growth strata in relation to fold growth [*Burbank et al*., 1996]. This interpretation on growth strata is based mainly on the observed stratigraphic contact relationship and changes in stratigraphic attitude. A true interpretation should be further evidenced by high-resolution subsurface data for this fold. Our new magnetostratigraphic study constrains the deposition of growth strata on the backlimb of the Saerqiaoke anticline at circa 6.4 Ma (Figure 5), suggesting the initiation of the anticlinal growth around the same age. More detailed insight on the anticlinal growth emerges from analysis of the sediment-accumulation rate curve of the URS (Figure 6). As shown in Figure 6, the magnitude of the reduction in accumulation rate at ~6.1 and ~4.1 Ma is striking: about 15% and 50% decreases, respectively. In general, reduction of sediment accumulation across the anticlinal crest would be expected in response to accelerating crestal uplift [*Burbank et al*., 1996]. Given the position of the URS close to the anticlinal core (Figure 10b), we tentatively interpret the reductions of accumulation rate at ~6.1 and ~4.1 Ma observed in the URS as indicative of synchronous significant folding and uplift of the Saerqiaoke anticline.

The interpreted ~6 Ma tectonic event in the southern Chaiwopu Basin is nearly synchronous with deformation observed in the other sites of the Tian Shan [e.g., *Huang et al*., 2006; *Wang et al*., 2008; *Sun et al*., 2009; *Lu et al*., 2010a], the Pamir [e.g., *Thiede et al*., 2013; *Thompson et al*., 2015], the Kunlun Shan [e.g., *Zheng et al*., 2000; *Sun et al*., 2008], and the northeastern Tibetan Plateau [e.g., *Fang et al*., 2004, 2007; *Li et al*., 2014]. In foreland basins of the Tian Shan, acceleration of sediment-accumulation rate and growth strata [*Huang et al*., 2006; *Sun et al*., 2009; *Lu et al*., 2010a] and structural analysis [*Wang et al*., 2008] likewise identify the ~8–6 Ma uplift of the Tian Shan range and its resultant basinward encroachment. In the northern Kunlun Shan foreland, lithofacies changes and an increase in sediment-accumulation rate occurring at circa 4.5 Ma are regarded as indicative of synchronous uplift of the northwestern Tibetan Plateau [*Zheng et al*., 2000]. A similar result from *Sun et al*. [2008] constrains

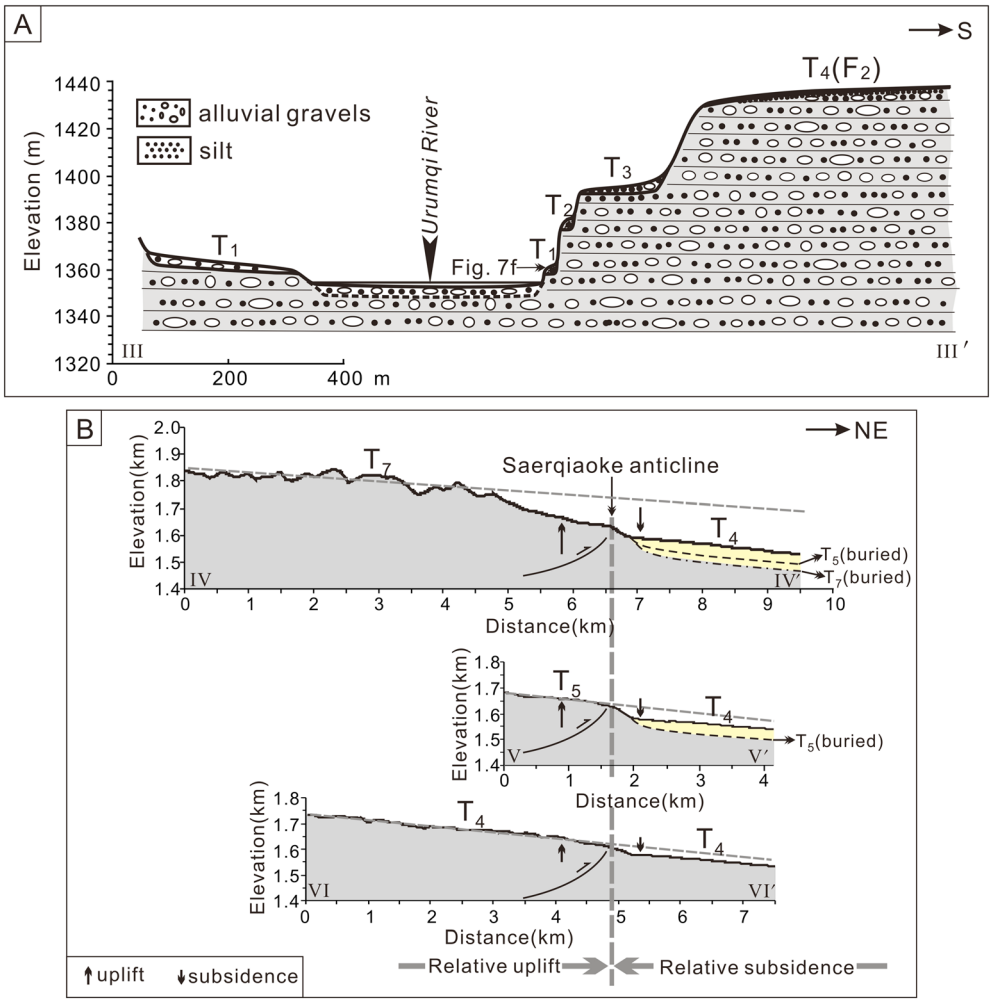

Figure 8. (a) Terrace to river cross section III-III′ of the Urumqi River based on the field investigations. Note that terrace deposits of all the three younger terraces T_1 to T_3 overlie the conglomerates of fan F_2. See Figure 1c for the location of this section. (b) The longitudinal profiles of terraces T_7 (IV-IV′), T_5 (V-V′), and T_4 (VI-VI′) (modified from *Lu et al.* [2014]) displaying sequential increase of deformation. See Figure 1c for the locations of these terrace longitudinal profiles.

the tectonic uplift of the Kunlun Shan at circa 5.3 Ma by magnetostratigraphic data on growth strata. On the northern front of the Qilian Shan in the northeastern Tibetan Plateau, the development of syntectonic deposition (growth strata) implies the growth and uplift of the range at circa 8 and 6.6 Ma [*Fang et al.*, 2004; *Li et al.*, 2014]. These above studies suggest that the ~8–6 Ma tectonic uplift is likely a regionally extensive, rather than a local event in the Asian interior. More deformation ages throughout the mountain belt help to better constrain this regional event. When considering that deformation in the Asian interior has progressively propagated into foreland areas through time, the ~8–6 Ma tectonic uplift should be a part of the overall propagation pattern. The uplifted topography resulting from the ~8–6 Ma event might have blocked the moisture transport of Westerlies and Indian Monsoon [e.g., *Miao et al.*, 2012] and thus have contributed to stepwise aridification in the Asian interior since ca. 6 Ma [e.g., *Miao et al.*, 2012; *Lu et al.*, 2013b].

6.2. Quaternary Deformation Revealed by Geomorphic Data

Subsequent growth and uplift of the Saerqiaoke anticline can be inferred from the intense accumulation in the southern Chaiwopu Basin. Basinward thrusting and propagation of the Tian Shan along the JFTF could have caused the uplifted topography of the Urumqi River catchment basin relative to the lowland Chaiwopu Basin [*Lu et al.*, 2014]. As a result, high-energy river systems enhanced erosion and transport. Vast amounts of clastic sediments were transported by the Urumqi River from the range into the southern

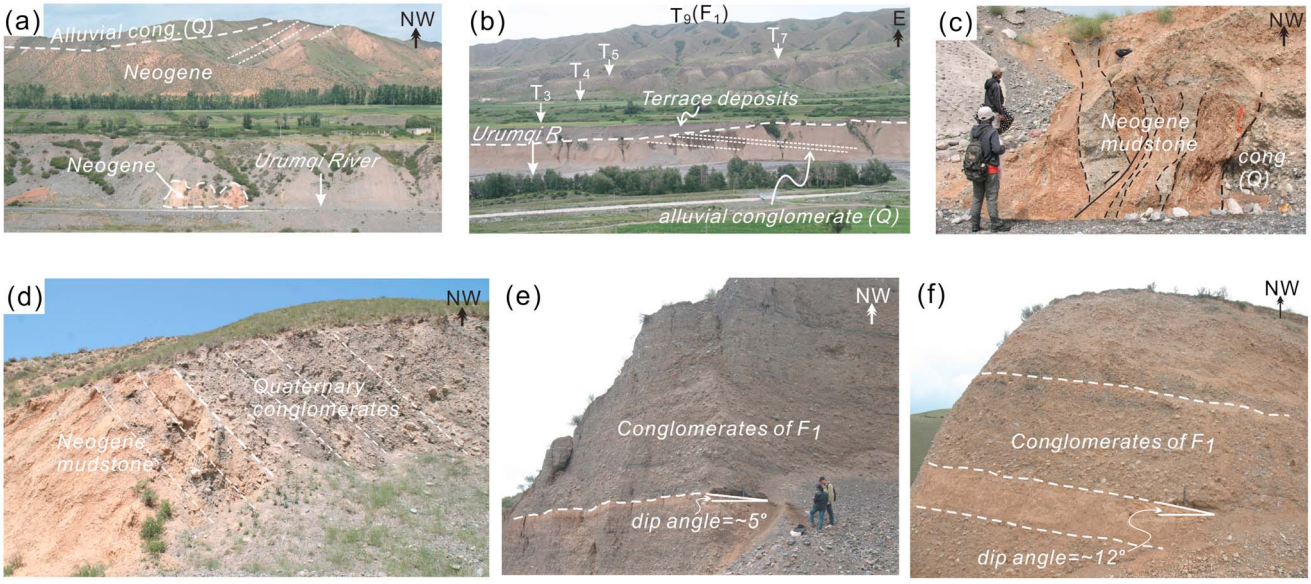

Figure 9. Photos showing the systematic changes in the stratigraphic attitudes across the Saerqiaoke anticline in the southern Chaiwopu Basin. Note that the alluviums in Figure 9e, dip approximately to the north with angle of about 5° but in Figure 9f where the elevation decreases by about 100m in comparison with the site of Figure 9e, the dip angle increases to about 12°. See Figure 1c for the locations and view directions of photos

Chaiwopu Basin and formed the mega alluvial fan F_1 (Figure 1c). The accumulation of alluvial sediments of F_1 ended at about 0.55 Ma due to river incision [*Lu et al.*, 2014]. Such incision has been regarded as a response to growth and rock uplift of the Saerqiaoke anticline caused by northward thrusting of the NSCF (Figure 10) [*Lu et al.*, 2014]. Therefore, we suggest anticlinal growth in the southern Chaiwopu Basin at circa 0.55 Ma. It is worth noting the change in attitudes of the alluviums in the proximal part of fan F_1, where the alluvium dips to the north in contrast to the stratigraphic attitudes in the southern limb of the Saerqiaoke anticline, with the lower (older) alluviums displaying steeper dips (Figures 9e, 9f, and 10b). Given that original attitude of alluvium deposited along mountain front is commonly characterized by a relatively gentle dip of a few degrees, this observation on bedding attitudes (Figures 9e, 9f, and 10b) seems to indicate the activation of the JFTF when the alluviums of F_1 deposited.

The more recent deformation of the Saerqiaoke anticline is revealed by the deformed terraces. As described in section 5, the younger terraces record less deformation (Figure 8b). Undoubtedly, this geometry implies continuous anticlinal growth since the abandonments of terraces T_7, T_5, and T_4. More detailed insight on deformation is from analysis of the young terrace T_1^H above the core of the Saerqiaoke anticline (Figures 1c and 7b). The terrace height profile indicates that terrace T_1^H has been vertically offset about 0.6 m by the thrust since its formation at about 7 Ka, defining the rate of deformation of 0.09 mm/yr. In comparison with the Holocene vertical rate of ~1 ± 0.3 mm/yr on the Tugulu-Dushanzi thrust in the western part of the northern Chinese Tian Shan foreland [*Avouac et al.*, 1993], this rate estimation is likely to indicate the relatively low activity of the NSCF during the Holocene in the southern Chaiwopu Basin, a piggyback basin in the easternmost part of the foreland. More geomorphologic data are needed to further constrain the tectonic activity in this area.

Basinward propagation of the Tian Shan along the JFTF is capable of resulting in a more steepened river gradient leading to overall downcutting into the old alluviums and thus yielding younger terraces [*Lu et al.*, 2010b]. Our field observations of the geomorphology (Figures 7c to 7f and 8a) support this idea. About 10 km northeast of the distal end of F_1 (Figure 1c), the terrace deposits of the three younger terraces (T_1 to T_3) overlie the conglomerates of fan F_2 (Figures 7c to 7f and 8a), suggesting the transition from deposition to downcutting of the Urumqi River since the abandonment of the surface of fan F_2. Therefore, we tentatively propose that formations of the three young terraces T_3 to T_1 were forced to some extent by the regional uplift in the southern Chaiwopu Basin due to basinward propagation of the Tian Shan. Certainly, climate change during glacial-interglacial cycles is also an important factor forcing river downcutting and terrace formation

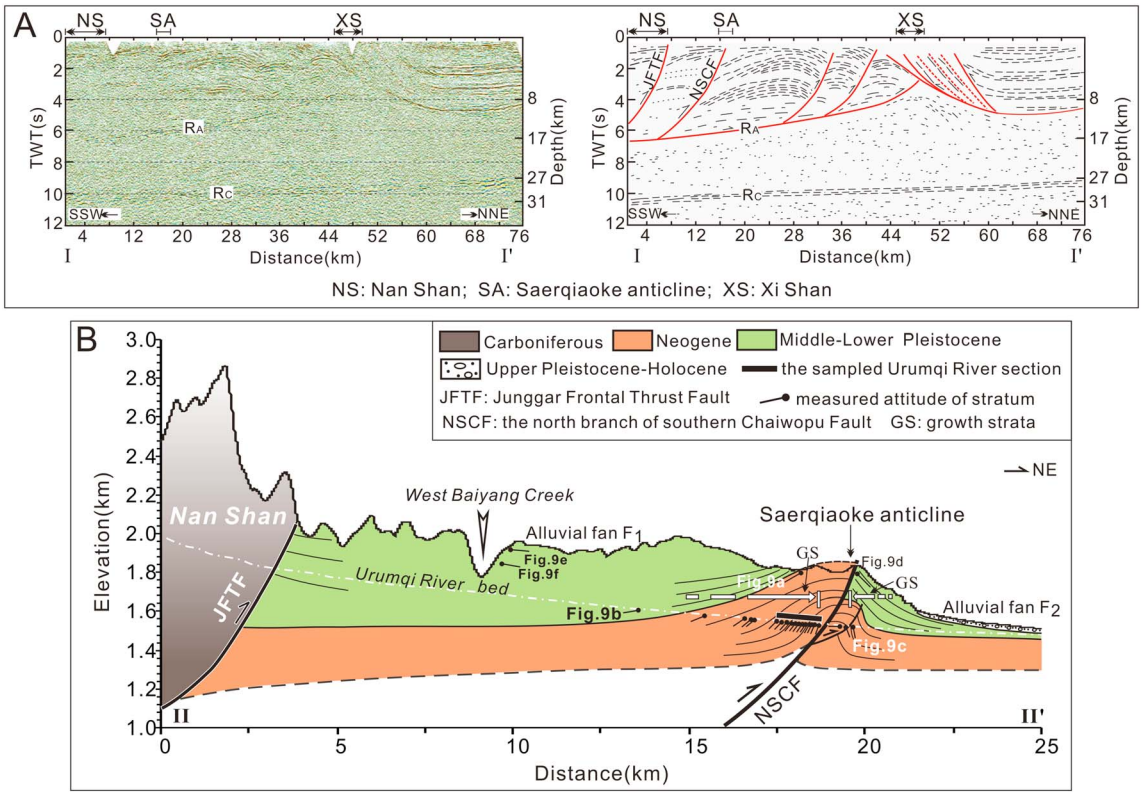

Figure 10. (a) Deep seismic reflection profile I-I′ stretching from the Nan Shan northward the Xi Shan (left) and the geological interpretation (right) (modified from *Liu et al*. [2007]). The dipping southward faults and the detachment horizon R_A, which is located at a depth of ~17–18 km (TWT: two-way traveltime 6.5 S) at the southern end of the seismic profile [*Liu et al*., 2007], compose a typical thrust nappe. R_C is a deeper detachment horizon gently dipping southward. See Figure 1b for the location of this seismic reflection profile. (b) II-II′ geological cross section along the course of the Urumqi River in the southern Chaiwopu Basin. The upper-lower Pleistocene conglomerates were deposited as a wedge-shaped depositional unit with the maximum thickness of about 400 m at the fanhead of alluvial fan F_1 [*Zhou et al*., 2002]. The thickness of the Neogene strata is unknown. The topography of this cross section is extracted from Google Earth images. The measured stratigraphic attitudes are shown at the measuring sites to exhibit the systematic changes in stratigraphic attitude in the southern Chaiwopu Basin. See Figure 1c for the location of this section.

[e.g., *Molnar et al*., 1994; *Pan et al*., 2003; *Lu et al*., 2010b, 2014; *Owen et al*., 2014]. Here we cannot eliminate the possible contribution of climate change to formations of terrace T_3 to T_1. We aim to collect more data on the alluvial sequence in order to better understand the relationship between terrace formation, tectonic uplift, and climate variation in the present study area.

7. Conclusions

In the southern Chaiwopu Basin of the northern Chinese Tian Shan foreland, the Urumqi River has incised deeply into the basement rocks and its overlying basin fill, thus yielding well-exposed outcrops of late Neogene-Quaternary terrigenous strata and well-developed Quaternary alluvial sequences. The systematic change in bedding dips displays a characteristic wedge-shaped stratigraphic geometry of the strata comprising Saerqiaoke's southern limbs, a small-scale structure developing at the distal end of the oldest alluvial fan F_1 of the Urumqi River. This observation is interpreted to indicate the existence of growth strata on the fold's southern limb. A new magnetostratigraphic study dates the basal age of growth strata to about 6.4 Ma, when folding of the Saerqiaoke anticline commenced due to basinward propagation of the Tian Shan. The resulting intense alluviation in the southern Chaiwopu Basin ceased around 0.55 Ma in response to significant uplift of the Saerqiaoke anticline and the resultant downcutting. Folded terraces record more recent tectonic deformation of this fold. The terrace height profile indicates that terrace T_1^H has been vertically offset about 0.6 m by thrust faulting since its formation at about 7 Ka. Basinward encroachment of the fold and thrust belts in both the northern and southern Tian Shan foreland is a crucial geological process accommodating Cenozoic crustal shortening within the India-Eurasia convergent system. The stratigraphic and geomorphic

data presented in this work are helpful to understand initiation of thrust-related folding in the northern Chinese Tian Shan foreland in relation to such a geological process. Future work will focus on quantification of fold growth rates using geologic and geomorphic data in the present study area.

Acknowledgments

This study was supported by the Natural Science Foundation of China (grants 41371031 and 41001002). The data of this paper are available at the School of Geographic Sciences, East China Normal University. Honghua Lu can be contacted for access to the data. Shiji Chen and Hao Wang are appreciated for their field assistances. We thank Jie Chen, Shihu Li, and Weiguo Zhang for their assistances in paleomagnetic analyses. Burbank Douglas W. is especially appreciated for his thoughtful comments, suggestions, and help with the English. J. Thompson and the other anonymous reviewer and the editor P. Tregoning are greatly appreciated for their constructive comments and language improvements on an earlier manuscript, which resulted in the great improvement of this manuscript.

References

Allen, M. B., B. F. Windley, C. Zhang, Z. Y. Zhao, and G. R. Wang (1991), Basin evolution within and adjacent to the Tien Shan Range, NW China, *J. Geol. Soc.*, *148*(2), 369–378.

Avouac, J.-P., P. Tapponnier, P. Bai, M. You, and G. Wang (1993), Active thrusting and folding along the northern Tien Shan and late Cenozoic rotation of the Tarim relative to Dzungaria and Kazakhstan, *J. Geophys. Res.*, *98*(B4), 6755–6804, doi:10.1029/92JB01963.

Bullen, M. E., D. W. Burbank, and J. Garver (2003), Building the northern Tien Shan: Integrated thermal, structural, and topographic constraints, *J. Geol.*, *111*, 149–165.

Burbank, D. W. (1992), Causes of recent Himalayan uplift deduced from deposited patterns in the Ganges basin, *Nature*, *357*, 680–683.

Burbank, D. W., and R. S. Anderson (2011), *Tectonic Geomorphology*, 2nd ed., pp. 17–44, John Wiley, Chichester, U. K.

Burbank, D. W., A. Meigs, and N. Brozović (1996), Interactions of growing folds and coeval depositional systems, *Basin Res.*, *8*, 199–223.

Burchfiel, B. C., E. T. Brown, Q. Deng, X. Feng, J. Li, P. Molnar, J. Shi, Z. Wu, and H. You (1999), Crustal shortening on the margins of the Tien Shan, Xinjiang, China, *Int. Geol. Rev.*, *41*(8), 665–700.

Butler, R. L. (1992), *Paleomagnetism*, Blackwell Sci. Publ., Cambridge, Mass.

Charreau, J., Y. Chen, S. Gilder, S. Dominguez, J.-P. Avouac, S. Sen, D. Sun, Y. Li, and W. Wang (2005), Magnetostratigraphy and rock magnetism of the Neogene Kuitun He section (northwest China): Implications for late Cenozoic uplift of the Tianshan mountains, *Earth Planet. Sci. Lett.*, *230*(1–2), 177–192.

Charreau, J., S. Gilder, Y. Chen, S. Dominguez, J.-P. Avouac, S. Sen, M. Jolivet, Y. A. Li, and W. M. Wang (2006), Magnetostratigraphy of the Yaha section, Tarim Basin (China): 11 Ma acceleration in erosion and uplift of the Tian Shan Mountains, *Geology*, *34*(3), 181–184.

Chen, J., D. W. Burbank, K. M. Scharer, E. Sobel, J. Yin, C. Rubin, and R. Zhao (2002), Magnetochronology of the upper Cenozoic strata in the Southwestern Chinese Tian Shan: Rates of Pleistocene folding and thrusting, *Earth Planet. Sci. Lett.*, *195*(1–2), 113–130.

Chen, J., R. Heermance, D. W. Burbank, K. M. Scharer, J. J. Miao, and C. S. Wang (2007), Quantification of growth and lateral propagation of the Kashi anticline, southwest Chinese Tian Shan, *J. Geophys. Res.*, *112*, B03S16, doi:10.1029/2006JB004345.

DeCelles, P. G., and K. A. Giles (1996), Foreland basin systems, *Basin Res.*, *8*, 105–123.

Deng, Q. D., X. Y. Feng, P. Z. Zhang, X. W. Xu, X. P. Yang, S. Z. Peng, and J. Li (2000), *Active Tectonics of the Tian Shan Mountains* [In Chinese], 399 pp., Seismology Press, Beijing.

Dupont-Nivet, G., W. Krijgsman, C. G. Langereis, H. A. Abels, S. Dai, and X. M. Fang (2007), Tibetan plateau aridification linked to global cooling at the Eocene–Oligocene transition, *Nature*, *445*, 635–638.

Fang, X. M., Z. J. Zhao, J. J. Li, M. D. Yan, B. T. Pan, C. H. Song, and S. Dai (2004), Magnetostratigraphy of late Cenozoic sediments of the Lao Jun Miao Anticline in the north margin of the Qilian Shan: Implication for the uplift of the northern Tibetan Plateau [In Chinese], *Sci. China, Ser. D: Earth Sci.*, *34*(2), 97–106.

Fang, X. M., W. L. Zhang, Q. Q. Meng, J. P. Gao, X. M. Wang, J. King, C. H. Song, S. Dai, and Y. F. Miao (2007), High resolution magnetostratigraphy of the Neogene Huaitoutala section in the eastern Qaidam Basin on the NE Tibetan Plateau, Qinghai Province, China and its implication on tectonic uplift of the NE Tibetan Plateau, *Earth Planet. Sci. Lett.*, *258*(1-2), 293–306.

Fisher, R. A. (1953), Dispersion on a sphere, *Proc. R. Soc. London*, *217*, 295–305.

Fu, B., A. Lin, K.-I. Kano, T. Maruyama, J. Guo, and K. Y. Abdrakhmatov (2003), Quaternary folding of the eastern Tian Shan, northern China, *Tectonophysics*, *369*, 79–101.

Gao, C. H. (2004), Sedimentary facies changes and climatic–tectonic controls in a foreland basin, the Urumqi River, Tian Shan, Northwest China, *Sediment. Geol.*, *169*, 29–46.

Heermance, R. V., J. Chen, D. W. Burbank, and C. S. Wang (2007), Chronology and tectonic controls of late Tertiary deposition in the southwestern Tian Shan foreland, NW China, *Basin Res.*, *19*, 599–632.

Heermance, R. V., J. Chen, D. B. Burbank, and J. Miao (2008), Temporal constraints and evidence for pulsed late Cenozoic deformation during the structural disruption of the active Kashi foreland, northwest China, *Tectonics*, *27*, TC6012, doi:10.1029/2007TC002226.

Hendrix, M. S., T. A. Dumitru, and S. A. Graham (1994), Late Oligocene–early Miocene unroofing in the Chinese Tian shan: An early effect of the India–Asia collision, *Geology*, *22*, 487–490.

Huang, B., J. D. Piper, S. Peng, T. Liu, Z. Li, Q. Wang, and R. Zhu (2006), Magnetostratigraphic study of the Kuche Depression, Tarim Basin, and Cenozoic uplift of the Tian Shan range, western China, *Earth Planet. Sci. Lett.*, *251*(3–4), 346–364.

Kirschvink, J. L. (1980), The least-squares line and plane and analysis of paleomagnetic data, *Geophys. J. Int.*, *62*(3), 699–718.

Li, H. M., H. T. Li, and C. L. Yu (1990), Quaternary magnetostratigraphy of Chaiwopu Basin, in *The Quaternary Climo–Environment Changes and Hydrogeological Condition of Chaiwopu Basin in Xinjiang Region* [In Chinese with English abstract], edited by Y. F. Shi, Q. Z. Wen, and Y. G. Qu, pp. 25–37, China Ocean Press, Beijing.

Li, J. J., X. M. Fang, C. H. Song, B. T. Pan, Y. Z. Ma, and M. D. Yan (2014), Late Miocene–Quaternary rapid stepwise uplift of the NE Tibetan Plateau and its effects on climatic and environmental changes, *Quat. Res.*, *81*(3), 400–423.

Li, T., J. Chen, J. A. Thompson, D. W. Burbank, and X. Yang (2013), Quantification of three-dimensional folding using fluvial terraces: A case study from the Mushi anticline, northern margin of the Chinese Pamir, *J. Geophys. Res. Solid Earth*, *118*, 4628–4647, doi:10.1002/jgrb.50316.

Liu, B. J., J. Shen, X. K. Zhang, Y. Chen, S. M. Fang, H. P. Song, S. Y. Feng, and C. B. Zhao (2007), The crust structures and tectonics of Urumqi depression revealed by deep seismic reflection profile in the northern margin of Tianshan Mountains [In Chinese], *Chin. J. Geophys.*, *50*(5), 1464–1472.

Lourens, L., F. Hilgen, N. J. Shackelton, J. Laskar, and D. Wilson (2004), The Neogene Period, in *A Geologic Time Scale*, edited by F. M. Gradstein, J. G. Ogg, and A. G. Smith, pp. 409–440, Cambridge Univ. Press, Cambridge, U. K.

Lu, H. H., D. W. Burbank, Y. L. Li, and Y. M. Liu (2010a), Late Cenozoic structural and stratigraphic evolution of the northern Chinese Tian Shan foreland, *Basin Res.*, *22*, 249–269.

Lu, H. H., D. W. Burbank, and Y. L. Li (2010b), Alluvial sequence in the north piedmont of the Chinese Tian Shan over the past 550 kyr and its relationship to climate change, *Palaeogeogr. Palaeoclimatol. Palaeoecol.*, *285*(3–4), 343–353.

Lu, H. H., Y. Chang, W. Wang, and Z. Y. Zhou (2013a), Rapid exhumation of the Tianshan Mountains since the early Miocene: Evidence from combined apatite fission track and (U–Th)/He thermochronology, *Sci. China Earth Sci.*, *56*(12), 2116–2125.

Lu, H. H., W. G. Zhang, Y. L. Li, C. Y. Dong, T. Q. Zhang, Z. Y. Zhou, and X. M. Zheng (2013b), Rock magnetic properties and paleoenvironmental implications of an 8–Ma late Cenozoic terrigenous succession from the northern Tian Shan foreland basin, northwestern China, *Global Planet. Change*, *111*, 43–56.

Lu, H. H., T. Q. Zhang, J. X. Zhao, S. P. Si, H. Wang, S. J. Chen, X. M. Zheng, and Y. L. Li (2014), Late Quaternary alluvial sequence and uplift-driven incision of the Urumqi River in the north front of the Tian Shan, northwestern China, *Geomorphology*, *219*, 141–151.

McElhinny, M. W. (1964), Statistical significance of the fold test in paleomagnetism, *Geophys. J. Int.*, *8*(3), 338–340.

McFadden, P. L., and M. W. McElhinny (1990), Classification of the reversal test in palaeomagnetism, *Geophys. J. Int.*, *103*, 725–729.

Meigs, A., D. W. Burbank, and R. A. Beck (1995), Middle-late Miocene (>10 Ma) formation of the Main Boundary thrust in the western Himalaya, *Geology*, *23*, 423–426.

Miao, Y. F., M. Herrmann, F. L. Wu, X. L. Yan, and S. L. Yang (2012), What controlled Mid-Late Miocene long-term aridification in Central Asia?—Global cooling or Tibetan Plateau uplift: A review, *Earth Sci. Rev.*, *112*, 155–172.

Molnar, P. (2001), Climate change, flooding in arid environments, and erosion rates, *Geology*, *29*(12), 1071–1074.

Molnar, P. (2004), Late Cenozoic increase in accumulation rates of terrestrial sediment: How might climate change have affected erosion rates?, *Annu. Rev. Earth Planet. Sci.*, *32*, 67–89.

Molnar, P., et al. (1994), Quaternary climate change and the formation of river terraces across growing anticlines on the north flank of the Tianshan, China, *J. Geol.*, *102*, 583–602.

Najman, Y., M. Pringle, L. Godin, and G. Oliver (2001), Dating of the oldest continental sediments from the Himalayan foreland basin, *Nature*, *410*, 194–197.

Owen, L. A., S. J. Clemmerns, R. C. Finkel, and H. Gray (2014), Late Quaternary alluvial fans at the eastern end of the San Bernardino Mountains, Southern California, *Quat. Sci. Rev.*, *87*, 114–134.

Pan, B. T., D. W. Burbank, Y. Wang, G. Wu, J. Li, and Q. Guan (2003), A 900 ky record of strath terrace formation during glacial-interglacial transitions in northwest China, *Geology*, *31*(11), 957–960.

Rees-Jones, J. (1995), Optical dating of young sediments using fine–grain quartz, *Ancient TL*, *13*(2), 9–14.

Reigber, C., G. W. Michel, R. Galas, D. Angermann, J. Klotz, J. Y. Chen, A. Papschev, R. Arslanov, V. E. Tzurkov, and M. C. Ishanov (2001), New space geodetic constraints on the distribution of deformation in Central Asia, *Earth Planet. Sci. Lett.*, *191*(1–2), 157–165.

Riba, O. (1976), Syntectonic unconformities of the Alto Cardener, Spanish Pyrenees: A genetic interpretation, *Sediment. Geol.*, *15*, 213–233.

Scharer, K. M., D. W. Burbank, J. Chen, and R. J. Weldon II (2006), Kinematic models of fluvial terraces over active detachment folds: Constraints on the growth mechanism of the Kashi–Atushi fold system, Chinese Tian Shan, *Geol. Soc. Am. Bull.*, *118*, 1006–1021.

Sobel, E. R., M. Oskin, D. W. Burbank, and A. Mikolaichuk (2006a), Exhumation of basement–cored uplifts: Example of the Kyrgyz Range quantified with apatite fission track thermochronology, *Tectonics*, *25*, TC2008, doi:10.1029/2005TC001809.

Sobel, E. R., J. Chen, and R. V. Heermance (2006b), Late Oligocene–Early Miocene initiation of shortening in the Southwestern Chinese Tian Shan: Implications for Neogene shortening rate variations, *Earth Planet. Sci. Lett.*, *247*, 70–81.

Sun, J. M., L. Zhang, C. Deng, and R. Zhu (2008), Evidence for enhanced aridity in the Tarim Basin of China since 5.3 Ma, *Quat. Sci. Rev.*, *27*, 1012–1023.

Sun, J. M., Y. Li, Z. Q. Zhang, and B. H. Fu (2009), Magnetostratigraphic data on Neogene growth folding in the foreland basin of the southern Tianshan Mountains, *Geology*, *37*(11), 1051–1054.

Suppe, J., G. T. Chou, and S. C. Hook (1992), Rates of folding and faulting determined from growth strata, in *Thrust Tectonics*, edited by K. R. McClay, pp. 105–121, Chapman and Hall, London.

Thiede, R. C., E. R. Sobel, J. Chen, L. M. Schoenbohm, D. F. Stockli, M. Sudo, and M. R. Strecker (2013), Late Cenozoic extension and crustal doming in the India-Eurasia collision zone: New thermochronologic constraints from the NE Chinese Pamir, *Tectonics*, *32*, 763–779, doi:10.1002/tect.20050.

Thompson, J. A., D. W. Burbank, T. Li, J. Chen, and B. Bookhagen (2015), Late Miocene northward propagation of the northeast Pamir thrust system, northwest China, *Tectonics*, *34*, 510–534, doi:10.1002/2014TC003690.

Vandenberghe, J., X. Wang, and H. Lu (2011), Differential impact of small-scaled tectonic movements on fluvial morphology and sedimentology (the Huang Shui catchment, NE Tibet Plateau), *Geomorphology*, *134*(3–4), 171–185.

Wang, S. L., Y. Chen, and H. F. Lu (2008), Growth of the Huoerguosi anticline (north Tianshan Mountains) by limb rotatioin since the late Miocene, *Chin. Sci. Bull.*, *53*(19), 3028–3036.

Wang, X. L. (2006), On the performances of the single–aliquot regenerative–dose SAR protocol for Chinese loess: Fine quartz and polymineral grains, *Radiat. Meas.*, *41*(1), 1–8.

Windley, B. F., M. B. Allen, C. Zhang, Z. Y. Zhao, and G. R. Wang (1990), Paleozoic accretion and Cenozoic redeformation of the Chinese Tien Shan Range, central Asia, *Geology*, *18*(2), 128–131.

Yang, J. C., and Y. L. Li (2011), *Active Tectonic Geomorphology* [In Chinese], Peking Univ. Press, Beijing.

Yang, K. M., J. C. Wu, E. W. Cheng, Y. R. Chen, W. C. Huang, C. C. Tsai, J. B. Wang, and H. H. Ting (2014), Development of tectonostratigraphy in distal part of foreland basin in southwestern Taiwan, *J. Asian Earth Sci.*, *88*, 98–115.

Yang, X. P., A. Li, and W. L. Huang (2012), Uplift differential of active fold zones during the late Quaternary, northern piedmonts of the Tianshan Mountains, China [In Chinese], *Sci. China Earth Sci.*, *42*(12), 1877–1888.

Yin, A., S. Nie, P. Craig, T. M. Harrison, F. J. Ryerson, X. Qian, and G. Yang (1998), Late Cenozoic tectonic evolution of the southern Chinese Tian Shan, *Tectonics*, *17*(1), 1–27, doi:10.1029/97TC03140.

Yu, S., W. Chen, N. J. Evans, B. I. A. McInnes, J. Y. Yin, J. B. Sun, J. Li, and B. Zhang (2014), Cenozoic uplift, exhumation and deformation in the north Kuqa Depression, China as Constrained by (U–Th)/He thermochronometry, *Tectonophysics*, *630*, 166–182.

Zhang, P. Z. (2004), Late Cenozoic tectonic deformation in the Tianshan Mountain and its foreland basins, *Chin. Sci. Bull.*, *49*(4), 311–313.

Zhang, P. Z., P. Molnar, and W. R. Downs (2001), Increased sedimentation rates and grain sizes 2–4 Myr ago due to the influence of climate change on erosion rates, *Nature*, *410*, 891–897.

Zheng, H., C. M. Powell, Z. An, J. Zhou, and G. Dong (2000), Pliocene uplift of the northern Tibetan Plateau, *Geology*, *28*(8), 715–718.

Zhou, S. Z., K. Q. Jiao, J. D. Zhao, S. Q. Zhang, J. X. Cui, and L. B. Xu (2002), Geomorphology of the Urumqi River valley and the uplift of the Tianshan Mountains in Quaternary [In Chinese], *Sci. China, Ser. D: Earth Sci.*, *32*(2), 157–163.

Zubovich, A. V., et al. (2010), GPS velocity field for the Tien Shan and surrounding regions, *Tectonics*, *29*, TC6014, doi:10.1029/2010TC002772.